The interaction between vacancies and twin walls, junctions, and kinks, and their mechanical properties in ferroelastic materials

Xiaomei He[1], Suzhi Li[1]*, Xiangdong Ding[1]*, Jun Sun[1],

Sverre M. Selbach[3], Ekhard K. H. Salje[1,2]*

[1] State Key Laboratory for Mechanical Behavior of Materials, Xi'an Jiaotong University, Xi'an 710049, China

[2] Department of Earth Sciences, University of Cambridge, Cambridge CB2 3EQ, United Kingdom

[3] Department of Materials Science and Engineering, NTNU Norwegian University of Science and Technology, N7491 Trondheim, Norway

E-mail: lisuzhi@xjtu.edu.cn; dingxd@mail.xjtu.edu.cn; ekhard@esc.cam.ac.uk

Abstract

Vacancies strongly interact with twin boundaries and often change dramatically the properties of a ferroelastic material. However, the understanding of this behavior at an atomic-level is still deficient. Here we study vacancy diffusion processes across very large length- and time-scales using a combination of molecular dynamics and Monte Carlo simulations. We find that vacancies reduce their energy by residing at twin boundaries, kinks inside domain boundaries, and junctions between domain boundaries. Vacancies have the largest binding energy inside junctions and co-migrate with the motion of the junctions. For the weaker trapping inside twin boundaries, a "ghost line" may be generated because vacancies do not necessarily diffuse with moving boundaries and are left behind, leaving a trace of a previous position of the domain boundary. Needle twins act as channels for fast diffusion with almost one order of magnitude higher vacancy diffusivity than in bulk. The relative concentration of vacancies at twin boundaries (ρ_{Va}) is a function of the average vacancy concentration (C_{Va}) with $\rho_{Va} \sim C_{Va}^{\alpha}$ and $\alpha = 0.61$, in contrast to that of immobile vacancies case with $\alpha = 0.4$. The concentration of vacancies at twin boundaries is enriched ca. 5 times at low temperatures. With increasing temperature, the enrichment drops as the trapping potential at the twin boundaries decreases (thermal release). The distribution of energy-drop upon twin pattern evolution follows a power law. The exponent ε increases from ~1.44 to 2.0 when the vacancy concentration increases. The power law exponent is the same in the athermal region, while Vogel-Fulcher behavior is found at high temperatures.

Keywords: Vacancy; Twin boundaries; Domain boundary engineering; Atomistic simulations

1 Introduction

Functional properties of ferroelastic materials rely largely on twin boundary movements. Shape memory alloys with their superelasticity and shape memory effects fall into the same class of materials. Their domain switching and domain wall (or twin boundary) motion dominate these effects. For example, Cu-Al-Ni nanopillars show a strong shape memory recoverability through twinning and de-twinning mechanisms, while this effect is destroyed by high densities of stacking faults in small size nanopillars [1]. In Ti-Ni-based shape memory alloys, the motion of twin boundary could improve fatigue resistance when the temperature is below the martensitic transition temperature [2]. Some metallic nanowires can even exhibit novel superelasticity with the aid of twin boundary motion [3-5].

Point defects and their interactions with twin boundaries (TBs) have great impact on the mechanical properties in ferroelastic materials as point defects usually pin twin boundary motion. Consequently, various mechanical properties change in the presence of point defects [6-10]. It is found that Cu-Al-Ni alloys have a 'normal' Young's modulus and small damping at temperature above ~ 220 K, but high damping at lower temperature [8]. The reason lies in the majority of TBs being pinned by 'Cottrell atmospheres' at low temperature [11]. As the temperature decreases, the mobility of defects becomes smaller, which results in a weaker pinning force and higher damping. In addition, the Ti-Ni-based shape memory alloys were observed to exhibit ultrahigh-damping behavior in the environment of hydrogen [12, 13]. The recoverability of shape memory alloys could also be affected by quenched-in point defects. When the twinned copper-based alloys, such as Cu-Zn-Al [14] and Cu-Al-Mn [15], are subjected to up-quenching, it is found that higher heating rates could promote the shape recovery (> 20 K/min). However, the recoverability is largely suppressed under low heating rates (~ 1 K/min) due to the strong pinning effect on slowly moving TBs by high concentration of mobile quenched-in vacancies. Besides, the martensitic phase transition temperature is found to decrease by a combination of thermal cycling and room temperature aging in Ni-rich Ni-Ti alloys, which is believed to originate from the interplay between the point defects and moving TBs [16, 17]. From a general viewpoint, changing the interactions between point defects and TBs is believed to be an effective means to tuning mechanical properties, which is known as domain boundary engineering [18].

Vacancies are an important type of point defects in crystals and will inevitably interact with twin boundaries. At room temperature, the thermal equilibrium concentration of vacancies is very low, but vacancies can also be generated under plastic deformation [19]. Several experimental studies have been carried out to understand the effect of

vacancies on the motion of TBs in $BiFeO_3$ with acceptor-oxygen-vacancy defect pairs [20], the mineral anorthoclase and a general case of ferroelastic walls with vacancies [21-23], in particular the memory effect of TBs due to pinning effect. A few simulations were performed to study this effect for perovskite structures [24-28]. Meanwhile, the vacancies could also act as nucleation sites for domain switching [29]. The interaction of vacancy with TBs often prompts vacancies assemblies at TBs [24], which may result in some novel and attractive properties on TBs, such as enhanced local conductivity [30, 31], polar ferroelastic TBs [32-35] and even a sheet superconducting phase along TBs in an insulating matrix [36-38]. Besides, oxygen vacancies through pinning TBs motion are known as a fatigue mechanism in ferroic materials [39, 40].

Although various studies have been carried out to study vacancy-TBs interactions, the microscopic mechanisms are still not fully understood, especially how the vacancies interact with steps inside twin boundary (kinks) and with intersections of two twin boundaries (junctions). In our previous work [29], we have studied the interaction of immobile vacancies with straight twin boundary in ferroelastic materials and found the vacancies could act as the sites for promoting domain wall (DW) nucleation. In the current work, we study the influence of mobile vacancies on the nucleation and migration of domain walls. To capture the diffusivity of vacancies, we combined Monte Carlo (MC) and Molecular dynamics (MD) methods to perform atomistic simulations. These simulations reveal the effect of long-range diffusion on the interactions with simple twin walls, kinks and junctions. We found that junctions are the energy-favored sites for trapping vacancies compared to kinks and straight twin boundaries. Twin boundaries act as fast channels for vacancy diffusion, similar to pipe diffusion of point defects in dislocation cores [41-43]. We further studied the accumulation of vacancies at twin walls and found that the concentration is significantly enhanced compared to the average concentration. Finally, we explore the statistics of the deformation process. The movement of twin boundaries with vacancies is non-smooth and progresses by jerks and avalanches, following a power law distribution. The power law exponent increases with increasing vacancy concentration.

2 Simulation Methods

Our atomistic simulations are based on the standard ferroelastic model with 4° shear angle [44, 45]. The potential $U(r)$ is composed of three interatomic interactions as the first-nearest harmonic interactions $U_{NN} = 20(r\text{-}1)^2\ (0.8 \le r < 1.2)$, the second-nearest double well interactions $U_{NNN} = -10(r - \sqrt{2})^2 + 2000(r - \sqrt{2})^4\ (1.207 \le r < 1.621)$ and the third-nearest fourth-order interactions $U_{NNNN} = -(r\text{-}2)^4\ (1.8 \le r < 2.2)$, where r is atomic

distance vector. Here we use a relatively high spring stiffness of 20 in U_{NN} in order to simplify the domain patterns [45, 46]. The equilibrium lattice constant a is set to be 1 Å and atomic mass M is 10 amu. Free boundary conditions are applied in the current 2D model. The system size is $500a \times 502a$, containing two pre-existing horizontal twin boundaries as the initial configuration. The ratio of the height of the switchable intermediate layer to the total sample is fixed to be 0.5.

Vacancies are randomly introduced in the middle layer of a sandwich model with different concentrations. The vacancy concentration C_{Va} is measured as the ratio of total number of vacancies to the total number of atoms in the system. C_{Va} ranges from 4 ppm to 500 ppm. The initial samples were relaxed with the conjugate gradient algorithm. Dynamic relaxations were then annealed at a given temperature ranging from $T = 5 \times 10^{-4} T_{\mathrm{VF}}$ to $T = 5.0 T_{\mathrm{VF}}$, where T_{VF} is the Vogel-Fulcher temperature. After relaxation, we adopted step loading and relaxing method by using a combined MD and MC techniques. Specifically, each step consists of one MD "fast" cold shear and tens of times MC "slow" vacancy diffusion for each loading step. For shearing, the external shear strain was applied via top and bottom fixed layers. The increment of shear strain in each loading step is 0.004%. The total number of loading-relaxing cycles is ~2500 and the total amount of strain is around 10%. The MC code is based on the Metropolis criterion and the number of MC attempts (N_{MC}) is proportional to the vacancy concentration C_{Va}. On average, each vacancy has five times attempts to diffuse in one loading cycle. Canonical ensemble (NVT) is used and the temperature is kept by a Nosé-Hoover thermostat [47, 48]. All the MD simulations were performed with the LAMMPS code [49] and the atomic configurations were displayed via AtomEye [50] and the Open Visualization Tool (Ovito) software [51].

3 Results

3.1 Formation of complex twin pattern upon shearing

We applied simple shear to the system with different amount of vacancies. Fig. 1(a) shows the stress-strain curves with vacancy concentration C_{Va} ranging from 40 ppm (grey curve) to 500 ppm (blue curve) in atomic ratio. In the following, we take the sample with C_{Va} = 400 ppm to illustrate our results. After the elastic state, the system starts to yield and then undergoes a long stage of plastic deformation region with weak strain hardening. The inset in Fig. 1 shows the variation of the yield point with the vacancy concentration. The yield point decreased with increasing vacancy concentration C_{Va}. Fig. 1(b) and 1(c) shows the atomic configurations of point A and B. Needle twins nucleate at the yield point A, followed by the yield collapse from point A to B. For clarity, the red dots mark the vacancies diffusing to twin boundaries. Domain

patterns form at the lower yield point B and display several vertical and horizontal twin walls. The twin pattern evolves intermittently under external shear strain (B-C). The preset horizontal domain finally switches its orientation by the de-twinning process and the whole sample becomes a single domain when the strain reaches the point C.

During the mechanical deformation, there are three kinds of defects formed: horizontal or vertical twin boundaries, kinks and junctions. The horizontal twins nucleate from free surfaces, while needle twins usually nucleate from the boundaries of horizontal twins. The movement of these twin boundaries relies on the nucleation and propagation of kinks. The intersections between horizontal and vertical twin boundaries form junctions. These junctions are stable and only move during the evolution of twin patterns, while kinks are known to have high mobility [52].

The vacancy concentration affects the complexity of domain patterns. As we manifested in our early work [29], vacancies can act as nucleation sites for twin boundaries. Moreover, the domain patterns become more complex as the vacancy concentration C_{Va} increases.

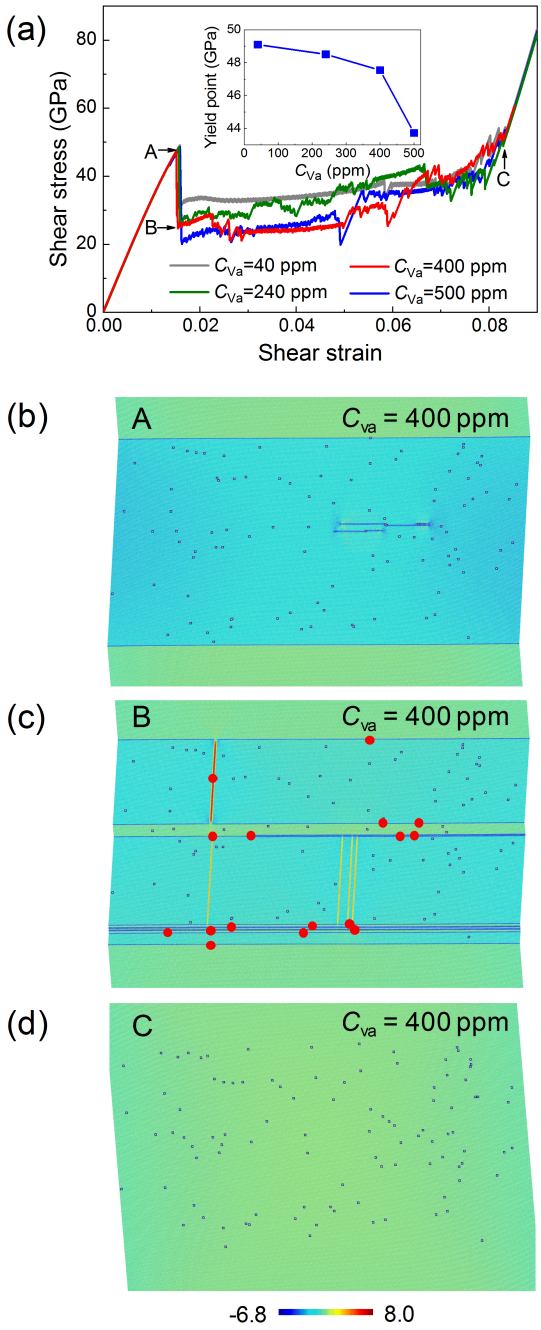

Fig. 1. (a) The shear stress versus shear strain with different vacancy concentrations C_{Va} ranging from 40 ppm to 500 ppm at $T = 5\times10^{-4}T_{VF}$. C_{Va} is measured as the ratio of total number of vacancies to the total number of atoms in the system. Points A, B and C mark the upper yield point, lower yield point and the termination of the plateau, respectively. The inset shows the dependence of yield point on the C_{Va}. A-B and B-C denote the yield region and the plastic region. (b)-(d) The atomistic configurations at point A, B and C marked in (a) with of C_{Va} = 400 ppm. Red dots mark vacancies in walls for clarity. Vacancies nucleate needle twins firstly at the yield point A. A complex twin pattern is formed in point B. The domain completely switches by de-twinning at point C. The color bar refers to the local shear angles relative to the underlying bulk structure ($|\Theta_{vertical}|$-4°+$\Theta_{horizontal}$), where $\Theta_{vertical}$ and $\Theta_{horizontal}$ refer to the vertical and horizontal angles respectively.

3.2 The binding energy of vacancy with various kinds of defects as twin boundaries, kinks and junctions

With the generation of various defects upon plastic deformation there will be several potential trapping sites for vacancies. Vacancies can cause local lattice distortions and thus produce local stress fields. These stress fields are approximately isotropic when the vacancy is isolated in the bulk, but highly anisotropic when the vacancy is located at a twin boundary or a junction. Fig. 2(a) shows the distribution of the potential energy of a vacancy located at twin boundaries, kinks and junctions, respectively. The formation of kinks in the twin boundary subtly changes the distribution of the potential energy while the potential energy shows three-fold symmetry close to a junction.

Fig. 2(b) shows the binding energy of vacancies near twin boundaries, kinks and junctions, which was calculated as the energy difference between a vacancy at a defect site and in the bulk as function of distance (r) to the core position of defects. The binding energy for vacancies at twin boundaries, kinks and junctions are $\Delta E_{\text{Va-TB}}$ = -0.014 eV, $\Delta E_{\text{Va-kink}}$ = -0.051 eV and $\Delta E_{\text{Va-junction}}$ = -0.114 eV right at the core position of defects (r = 0), respectively. From the energy differences it is evident that junctions deeply trap vacancies. The binding energy of Va-TBs calculated here is of the same order of magnitude with that obtained by some experiments and density functional theory (DFT) calculations. For example, the binding energy of oxygen interstitials and vacancies with neutral TBs are -0.03 eV [53] and +0.10 to +0.14 eV [54], respectively, in $YMnO_3$. In addition, oxygen vacancies have binding energies of -0.023 eV and -0.299 eV at TBs in $BaTiO_3$ and $PbTiO_3$, respectively [55].

To characterize the angular-dependent binding energy near kinks and junctions, we selected certain typical orientations to illustrate their variation as the function to distance with defects. The orientation is characterized as the rotation angle θ with respect to the vertical direction. We chose two directions for kinks (θ = 0° and 45°) and three directions for junctions (θ = 0°, 45° and 120°), as marked in Fig. 2(b). With the data, we further predict the profile of a twin wall by $y=y_0-B\,(\tanh(x/W))^2$, where x is the distance to the center position of defects and W is the half-width of interactions range [56, 57]. For the simple vacancy-TB interaction, 2W is 1.34 Å. For vacancy-kink interaction, the value of 2W along θ = 0° (blue points) and θ = 45° (red points) are 1.26 Å and 1.76 Å, respectively. For vacancy-junction interaction, the values of 2W for θ = 0° (black points) and θ = 120° (purple points) are almost the same with ~2.2 Å due to the three-fold symmetry. This is larger than 1.46 along θ = 45° (grey points).

Fig. 2(c) shows the effect of temperature on the binding energy. Owing to the low stability of kinks, we could only perform the calculation for interactions of vacancies

with twin boundaries and junctions. We find that when the temperature reaches $T = 3.0T_{VF}$, the energy of a vacancy at a twin boundary and a junction is very close to that in bulk. Large thermal fluctuation make these difference quite small and significantly suppress the trapping ability of twin boundaries.

We rationalize ours results as follow: the accumulation of vacancies at TBs, kinks and junctions is driven by the increase of configurational entropy when the distribution of the vacancies is randomised. We find that the change of vibrational entropy under heating is a smaller effect so that that configurational entropy will dominate only at higher temperatures. Increasing temperature also affects the enthalpic driving force favouring accumulation. The local strain fields at TBs, kinks and junctions arise from the discontinuous ferroelastic order parameter across these internal interfaces. The magnitude of the ferroelastic order parameter, or distortion mode amplitude, decreases with heating towards T_C in concordance with Landau theory [58]. Hence, the driving force for accumulation of vacancies at TBs, kinks and junctions is also expected to decrease upon heating in addition to the progressively more important configurational entropy contribution to the total energy of the system. This behavior is fully consistent with the results from our simulations.

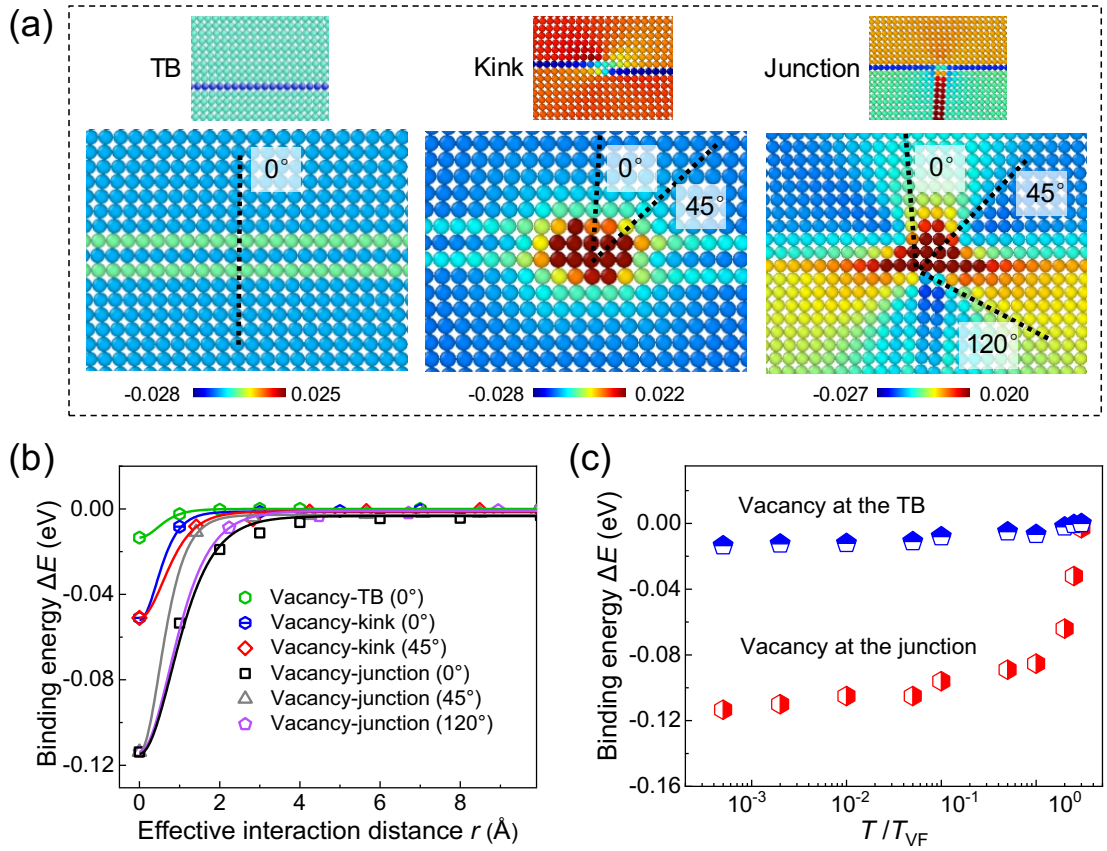

Fig 2. (a) The atomistic configurations for vacancies at twin boundary (left), kinks (middle) and junctions (right). The atoms are coded according to the potential energy. The upper-left inset of each

image shows twin boundary, kink and junction with colors coded by local shear angles ($|\Theta_{vertical}|$-4°+$\Theta_{horizontal}$). (b) The variation of binding energy of vacancy at twin boundary, kink and junction as the function to the core site of corresponding defects. The binding energy is defined as the potential energy difference of vacancy at twin boundary, kink and junction sites with the reference of that in bulk site. Specifically, the binding energies at the core position of defects are $\Delta E_{Va\text{-}TB}$ = -0.014 eV (green data), $\Delta E_{Va\text{-}kink}$ = -0.051 eV (blue and red data), and $\Delta E_{Va\text{-}junction}$ = -0.114 eV (grey, purple and black data) at r = 0 Å, respectively. Due to the orientation-dependent distribution of binding energy, we show the change of $\Delta E_{Va\text{-}kink}$ along 0° and 45° direction, and $\Delta E_{Va\text{-}junction}$ along 0°, 45° and 120° directions. (c) The effect of temperature on the binding energy of vacancy at twin boundary (blue points) and junctions (red points). When the temperature is above 3.0T_{VF}, the trapping ability of twin boundary almost vanishes.

3.3 Migration of vacancies with the movement of junctions

Figure 3 shows typical images of two cases where vacancies diffuse with the migration of the junction under shear loading. For case I (Fig. 3(a)-(c)), the vertical twin is very thin. When vacancies move very close to the junction they are trapped due to the elastic interactions. When the junction moves, a vacancy moves around 30 atomic layers with the junction. In Fig. 3I, the vacancy does not stay right at the junction but close-by; it is still dragged during the junction movement. For thicker vertical twins (case II), a vacancy is trapped right at the junction. It migrates instantly with the movement of the junction (Fig. 3(d)-(f)).

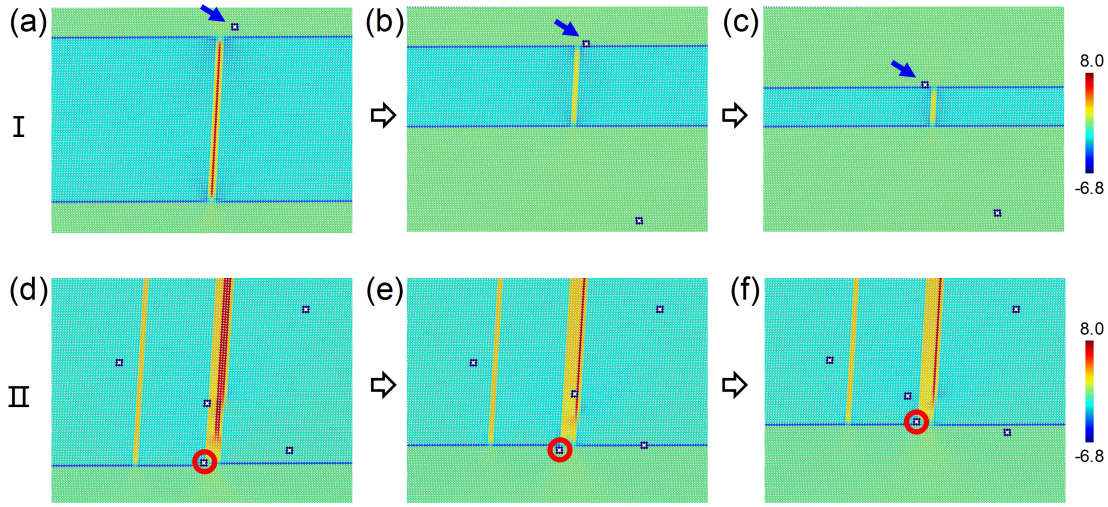

Fig. 3. Typical atomic images of vacancy diffusion during the migration of junctions. (a)-(c) Case I: the vacancy resides near the junction site. The vacancy is marked by blue arrow. (d)-(f) Case II: the vacancy is located at the junction site and moves with the junction. The red circles indicate the vacancy. The color of the atoms represents the local shear angles ($|\Theta_{vertical}|$-4°+$\Theta_{horizontal}$).

3.4 Formation of "ghost line"

Besides junctions, twin boundaries also trap vacancies. With long-time diffusion, vacancies diffuse onto the twin boundaries (Fig. 4(a)). The movement of twin boundaries is displacive under the external strain while the vacancy diffusion is a thermally activated process. Often, the mobility of twin boundaries is higher than vacancies and vacancies cannot follow the moving domain walls. We observe that when twin boundary move rapidly, vacancies are left behind at their previous sites (Fig. 4(b) and Fig. 4(c)). These vacancies aligned along such lines constitute "ghost lines". When observed by transmission electron microscopy, they appear like twin boundaries but there is no twinning - they constitute former twin boundaries, which have moved away. Such ghost lines are extremely common in minerals such as feldspar where defects moved onto twin boundaries at high temperatures. Under metamorphic conditions the twin boundaries moved but the temperature was too low for the defects to follow. They stay in their old position and form such ghost lines [23]. Analogous traces of electrically erased domain walls have been observed in $BiFeO_3$ and attributed to oxygen vacancies accumulated at the previous position of the wall. The presence of ghost lines depends on the binding energy between TBs and point defects like vacancies as well as the relative mobility of TBs and vacancies, where the TBs are usually significantly more mobile. If the binding energy is large and the mobilities of vacancies and TBs are similar, ghost lines will not appear as the vacancies will co-migrate with the TB. On the other hand, if the binding energy is small and/or the TB is more mobile than the vacancies, ghost lines will form upon movement of a TB [59]. At high temperatures the ghost lines are stable for a short time and will disappear by vacancy diffusion. This mechanism allows us to assess the thermal history of a sample, namely how long the sample was maintained at high temperatures without destroying the ghost lines. If a defect is located next to a junction, it is trapped much more strongly and moves with the junction (shown in Fig. 4(b) to Fig. 4(c) by the blue arrow).

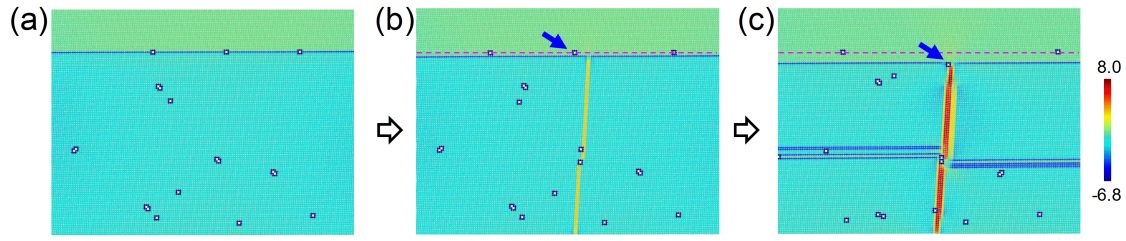

Fig. 4. (a)-(c) The atomistic configurations of "ghost line" formation. When a twin boundary moves, weakly trapped vacancies are left behind and form lines of defects at the sites of former twin boundaries. Only vacancies near the junction in (b) marked by a blue arrow migrate with the junction because their trapping is much deeper than in the wall. The color of the atoms refers to their local shear angles ($|\Theta_{vertical}|$-4°+$\Theta_{horizontal}$).

3.5 Vacancy diffusion along the twin boundary (pipe diffusion)

Twin boundaries accelerate the diffusive transport of vacancies along the boundary and reduce the diffusion out of the boundary (blue arrows in Fig. 5) [24, 60]. Here we only investigate rather narrow twin boundaries and even in this limit we observe a strong dependence on the thickness of the boundary. When the twin boundary thickness is two-atomic layers thick (or thicker), it acts as a fast channel to facilitate the migration of vacancies along the TBs. This effect is quite similar to pipe diffusion in a dislocation core, where dislocation lines act as fast channels for diffusion of point defects [41-43].

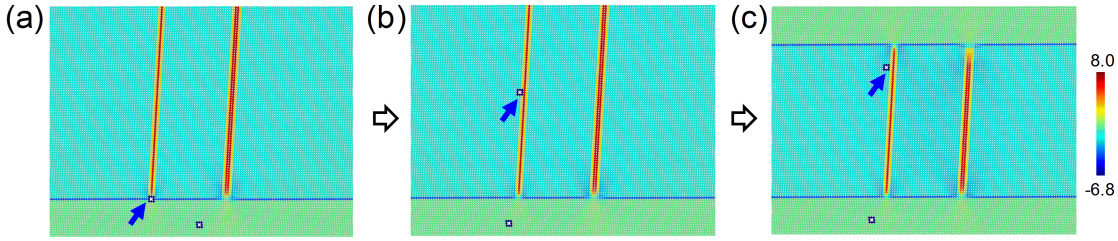

Fig. 5. Typical images of the diffusivity of vacancy along the twin boundary. The two-layers twin boundary acts as a channel for fast diffusion, similar to pipe diffusion of point defects in a dislocation core. The blue arrows indicate the vacancy position. The color of the atoms shows their local shear angles ($|\Theta_{vertical}|$-4°+$\Theta_{horizontal}$).

To assess the increase of the diffusivity inside the TBs, we calculated the diffusivity of vacancies in the bulk and along TBs by using our hybrid MD/MC methodology. Fig. 6(a) shows the mean squared displacement of vacancies with MC steps in the bulk at different temperatures. The diffusion coefficient D_{Va} of vacancies is calculated via the Einstein equation $D_{Va} = \langle r^2/(4t) \rangle$, where $\langle r^2 \rangle = 1/N \sum_1^N r_i^2$ is the mean squared displacement (MSD) of N vacancies for time t. We further calculate the diffusion coefficient D_{Va} by the Arrhenius law $D_{Va} = D_0 \exp(-\Delta E/(K_B T))$, where K_B is the Boltzmann constant, T is absolute temperature, and D_0 and ΔE are the pre-exponential factor and the activation energy for vacancy diffusion. For comparison, early experiments measured the Vogel-Fulcher temperature to be 230 K in $LaAlO_3$ [61], and the oxygen vacancy diffusion coefficient D_{Va} to be ca. 10^{-7}~$10^{-5.5}$ cm^2/s in the temperature range between 843 K and 1273 K [62]. To compare this with our simulations, each MC step would correspond to a real time t ~10 ps. Fig. 6(b) shows the variation of D_{Va} as the function of reciprocal temperature. By fitting the data linearly, we finally obtain the activation energy ΔE_{bulk} = 2.14 meV, as shown in Fig. 6(b). Fig. 6(c) shows the MSD for a vacancy diffusing along twin boundaries at different temperatures. We further calculated the activation barrier by fitting the data linearly and

obtained the activation barrier of $\Delta E_{TB} = 0.237$ meV for vacancy diffusing along twin boundaries. This activation energy is almost one order lower than that in the bulk and explains the pipe diffusion in TBs.

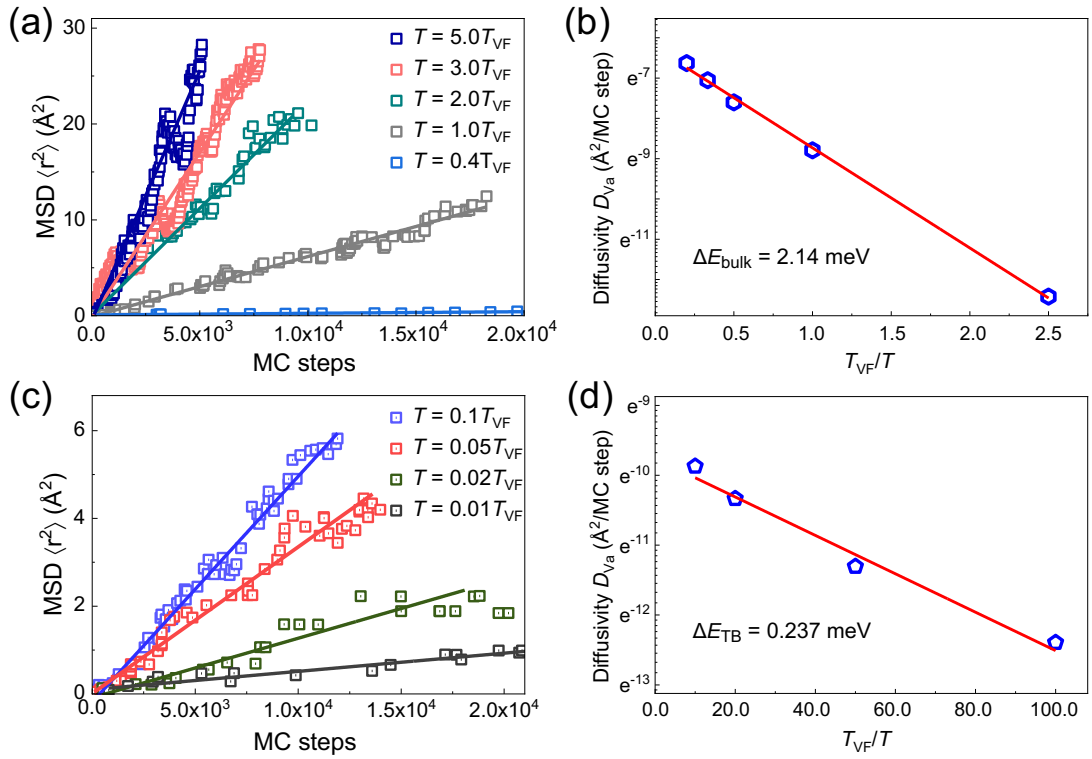

Fig. 6. Calculation of the vacancy diffusivity in bulk and twin boundaries. (a) Variation of the mean squared distance (MSD) of vacancy diffusion in the bulk at various temperatures. (b) The variation of $\ln(D_{Va})$ as the function of $1/T$ in the bulk. By fitting the data linearly, we obtain the activation energy to be 2.14 meV. (c) MSD of vacancies diffusing along the twin boundary at various temperatures. (d) The variation of $\ln(D_{Va})$ as the function of $1/T$ of vacancy diffusing around twin boundaries. The activation barrier is 0.237 meV.

4 Discussion

4.1 The relative concentration of mobile vacancies at the twin boundaries

Our results show that vacancies are trapped in junctions, kinks and twin boundaries with very different binding energies. We calculated the relative concentration of vacancies at these defects. The concentration ρ_{Va} is measured as the ratio of the total number of vacancies and the total number of atoms at the twin wall. Figure 7(a) shows the variation of ρ_{Va} with different amount of total vacancy concentration at $T = 5\times10^{-4}T_{VF}$ at the lower yield point B. The grey data refer to the concentration of immobile vacancies at twin boundaries. Naturally, owing to the enhanced diffusivity, the concentration of mobile vacancies is higher than that of immobile vacancies at

boundaries. The relative concentration of mobile vacancies at boundaries (ρ_{Va}) follows a power law distribution as a function of the average vacancy concentration C_{Va} as $\rho_{Va} \sim C_{Va}^{\alpha}$. With long-time diffusion, more and more vacancies will move onto walls [20]. Eventually the concentration should reach an equilibrium at which the rates of trapping and de-trapping of vacancies are the same. We probe the limit for the saturated concentration by relaxing the vacancies for a long time. The red data in Fig. 7(a) show equilibrium values of the relative vacancy concentration. The exponent of α is increased to 0.61, larger than 0.4 for immobile vacancies in twin boundaries. This means that the concentration is enhanced almost 5 times when $C_{Va} \geq 240$ ppm. Fig. 7(b) shows the twin boundary density ρ_{TB} as function of the average vacancy concentration C_{Va} at $T = 5\times10^{-4}T_{VF}$. We can see that the vacancies promote the nucleation of twins in so far as that the wall density increases with the increase of the vacancy concentration. However, driven by mechanical deformation, the density of twin boundaries under stress is less sensitive to the diffusivity of vacancies.

We also studied the influence of temperature on the variation of ρ_{Va}. Fig. 7(c) shows the value of ratio ρ_{Va}/C_{Va} at different temperature in the sample with $C_{Va} = 500$ ppm (see Supplementary materials). It drops as the temperature increases due to the reduction of trapping of vacancies at twin boundaries. The ratio decreases to ~2.45 at $T = 0.8T_{VF}$, indicating that TBs only weakly trap vacancies.

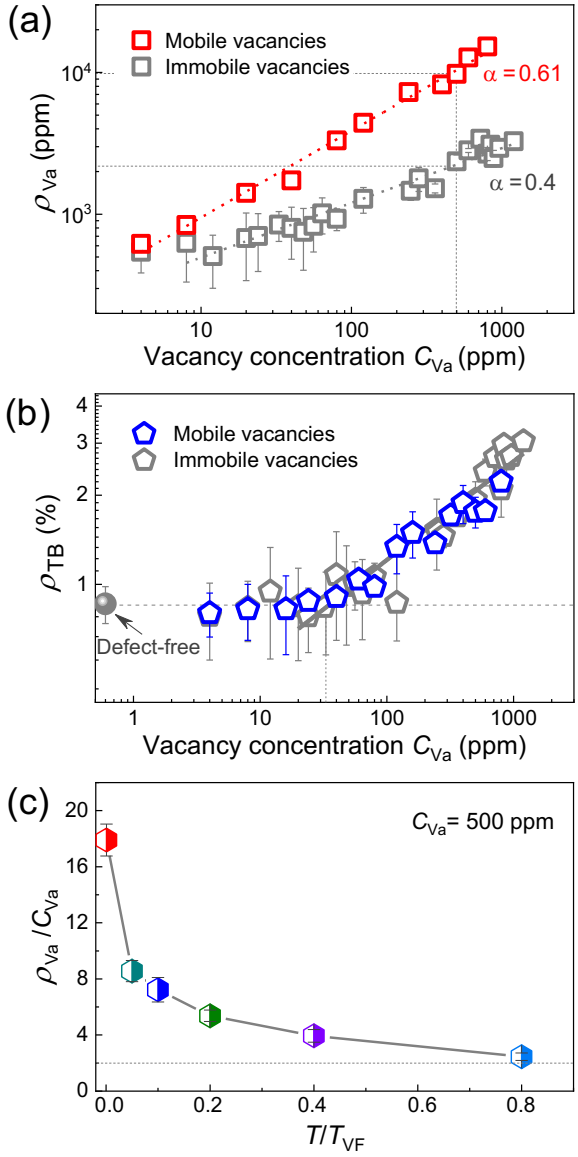

Fig. 7. (a) The relative concentration of vacancies at boundaries ρ_{Va} as function of the vacancy concentration C_{Va} at $T = 5\times10^{-4}T_{VF}$. For mobile vacancy after long time diffusion, it follows a power law $\rho_{Va} \sim C_{Va}^{\alpha}$ with $\alpha = 0.61$ (red data). The grey square is for the immobile vacancy with $\alpha = 0.4$ (see Ref. [29]). (b) The variation of twin boundary density ρ_{TB} with C_{Va} at $T = 5\times10^{-4}T_{VF}$ follows the power law relationship as $\rho_{TB} \sim C_{Va}^{\lambda}$ with $\lambda = 1/3$. The grey pentagon is for the immobile vacancy, and the error bars represent the standard deviation. ρ_{TB} shows a large variation at lower concentration when $C_{Va} < 100$ ppm. (c) The enrichment ratio of ρ_{Va}/C_{Va} decreases with increasing temperature and drops to 2.45 at $T = 0.8T_{VF}$.

4.2 The dynamics of twinning and de-twinning

4.2.1 Power law statistics

Our early work provided a statistical analysis of twinning-dominated deformation processes. We found power law distributions of yield collapse and plastic events in ferroelastic materials by MD simulations [46, 63]. Specifically, the distribution of jerk energy E is measured through the square of the strain e derivative of the potential energy U: $E = (dU/de)^2$ [44, 63, 64].

In the present study, because of some of jerk signals come from relaxation during the MC process, we use an energy-drop method to analyze the evolution of domain structures. Each data point of the potential energy curve is obtained by the potential energy change during step-loading deformation and afterwards relaxation process. The energy-drop $|\Delta U|$ is manifested by the drops between two adjacent data points in potential energy curve. Fig. 8(a) shows the energy-drop distribution of the yield and plastic regimes at $T = 5\times10^{-4}T_{VF}$. It follows a power law with $P(|\Delta U|) \sim |\Delta U|^{-\varepsilon}$. The exponent increases from 1.44 (defect-free system) to ~2.0 (C_{Va} = 400 ppm) and then remains constant [Fig. 8(b)]. The saturated value ~2.0 in systems with higher concentrations is lower than that of ~2.45 for immobile vacancies (marked by grey squares in Fig. 8(b)). The decrease of the exponent may be ascribed to the stronger pinning effect of twin boundaries by vacancies due to vacancy diffusion. The inset of Fig. 8(b) shows the maximum likelihood estimation of the more precise power-law exponents [65]. In order to evaluate the temperature effect, we calculated the energy-drop statistics for C_{Va} = 500 ppm in various temperatures range from $5\times10^{-4}T_{VF}$ to $0.4T_{VF}$. Fig. 8(c) shows the log-log plot for $P(|\Delta U|)$ and $|\Delta U|$. The corresponding exponent ε, determined by maximum likelihood method in Fig. 8(d), is about 1.95 ± 0.05 for each temperature. The exponent value ε is the same at different temperatures, indicating athermal behavior. An exponentially damped power law was found at higher temperatures with $T = 0.1T_{VF}$ and $0.4T_{VF}$ (orange points and blue points in Fig. 8(d), respectively). This damping stems from the energy loss of the migration of vacancies and high-frequency interactions between vacancies and twin walls.

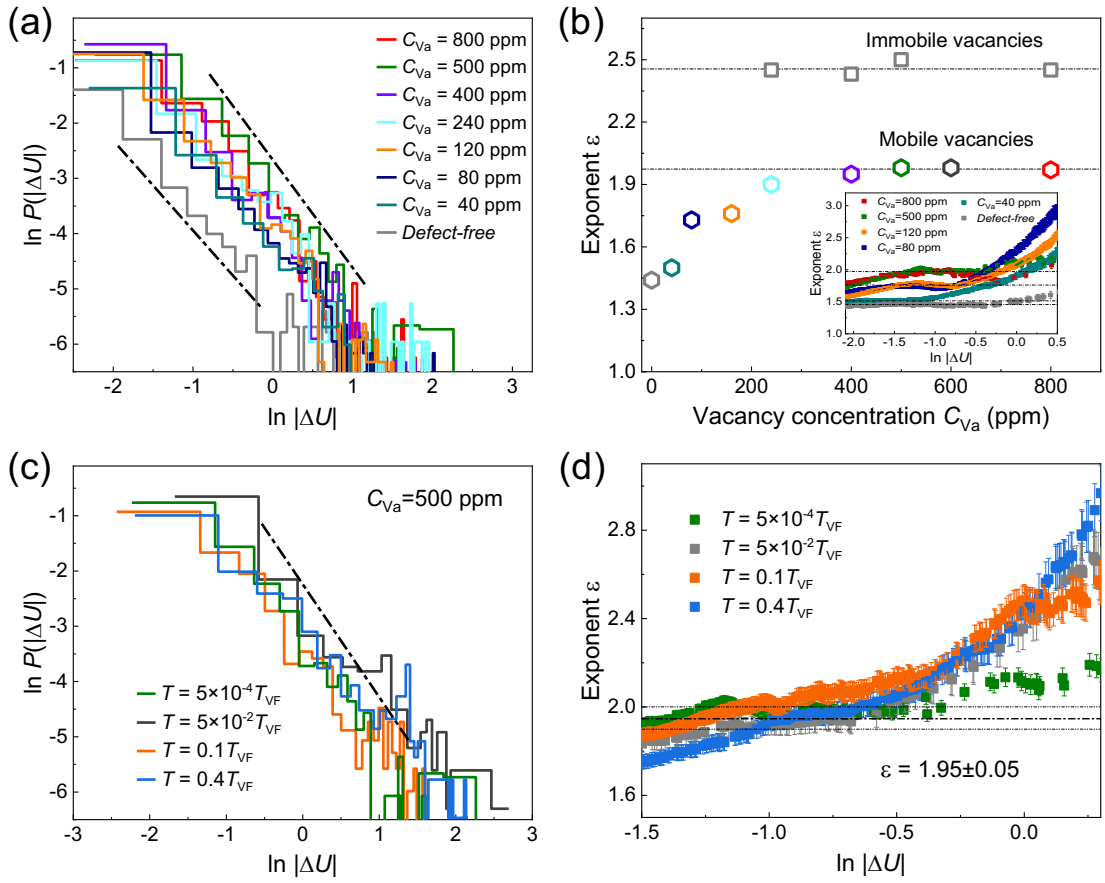

Fig. 8. The statistical analysis on the deformation process. (a) Probability distribution functions of the energy drops $P(|\Delta U|)$ in the yield and plastic regimes. It follows a power-law distribution $P(|\Delta U|) \sim |\Delta U|^{-\varepsilon}$ at $T = 5\times10^{-4}T_{VF}$. (b) The exponent ε increases slightly from 1.44 to 2.0 and then remains constant with increasing vacancy concentration. For immobile defects (grey squares), the exponent is 2.45 ± 0.05. Inset: the maximum likelihood method used for determining the exponents. (c) Power law distribution for C_{Va} = 500 ppm at different temperatures range from $5\times10^{-4}T_{VF}$ to $0.4T_{VF}$. (d) The corresponding exponent ε, evaluated by the maximum likelihood method, is around 1.95 for each temperature. The exponentially damping appeared at $T = 0.1T_{VF}$ and $0.4T_{VF}$.

4.2.2 Vogel-Fulcher behavior at high temperatures

The probability distribution function of energy-drop $P(|\Delta U|)$ follows the Vogel-Fulcher law $P(|\Delta U|) \sim \exp\text{-}(|\Delta U|/E_0)$ at high temperatures, where $E_0 \sim K_B(T\text{-}T_{VF})$ is corresponding to the activation energy, T_{VF} is the Vogel-Fulcher temperature, and K_B is the Boltzmann constant. Figure 9 shows the dependency of E_0 with T for systems containing mobile (red data) and immobile vacancies (blue data) with C_{Va} = 500 ppm. The activation energy increases greatly for mobile vacancies due to the stronger pinning effect. We then split the phase diagram into three typical regions. Regime I is the power-law region at low temperature. Regime III is the thermally activated region at high

temperature, and the parameter E_0 increases linearly at $T > T_{VF}$. The crossover between the regimes I and III follows stretched exponential statistics (regime II). By fitting the data linearly in the high-temperature region, we obtain T_{VF} = 10 K and 12 K for immobile and mobile systems, respectively. The black and blue vertical lines indicate the boundaries of these three distinct regions for mobile and immobile systems. We can see the temperatures at each boundary for mobile systems is a little higher than for immobile systems. In addition, we need to emphasize that in our previous study [29], T_{VF} is calculated to be 11 K by using the data of $(dU/de)^2$ for statistical analysis, where U and e are potential energy and strain. It is very close to the value obtained by energy-drop method used here.

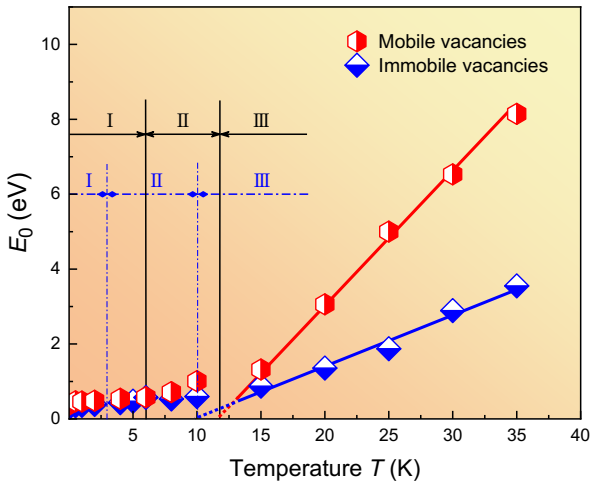

Fig. 9. Phase diagram for mobile and immobile vacancies systems as a function of temperature with C_{Va} = 500 ppm. E_0 is defined as $E_0 \sim K_B(T\text{-}T_{VF})$, which is corresponding to the activation energy. Vogel-Fulcher temperature (T_{VF}) is fitted to be 12 K and 10 K for mobile and immobile vacancy system, respectively. The energy-drop distribution $P(|\Delta U|)$ follows power law in regime I and follows Vogel-Fulcher statistics when temperatures $T > T_{VF}$ (regime III). The crossover between the power law regime and the thermally activated regime follows stretched exponential statistics (regime II).

4.3 Comparison of simulation results with experimental observations

In the following, we present several experimental studies providing indirect evidence of vacancy-twin boundary interaction effects on mechanical properties in ferroelastic materials. We compare our simulation results with experimental observations with respect to Young's modulus, shape recoverability and vacancy diffusivity.

In Cu-Al-Ni alloys, Young's modulus has been observed to exhibit a notable anomalous increase along with temperature-dependent internal friction in the range between approximately 220 K and 70 K [8]. Such behaviors result from the interactions between

point defects and mobile twin boundaries. These observations of Cu-Al-Ni alloys clearly show that atmospheres of defects produce a stronger pinning effect on twin boundaries than immobile or frozen defects. This observation is born out by our simulations. Similar effects have also been observed in other Cu-based martensites (Cu-Zn-Al [66] and Cu-Al-Be [67]) and in twinned ferromagnetic Ni-Fe-Ga [68] shape memory alloys.

Some experiments have shown that the recoverability is strongly suppressed by decreasing heating rate, as reported for Cu-Zn-Al shape memory alloy [14, 15]. It is found that the quenched Cu-based alloys could achieve ~90% shape recovery at high heating rate (~ 20 K/min), while only 10% is completed at a rate of 1 K/min. The strong interaction between quenched-in vacancies and phase boundaries is proposed as the reason for this behavior. Our current simulations support this point that when more and more vacancies are trapped at the twin boundaries after a long relaxation time (analogous to a very low heating rate), the pinning effect is much stronger. In addition, our statistical analysis shows that the Vogel-Fulcher temperature for mobile vacancies is higher than that of immobile systems (Fig. 9), which also indicates that de-pinning needs to overcome a higher barrier.

The diffusivity of point defects along twin walls was observed to differ from that of the bulk experimentally. For example, by doping Na into twinned crystals of WO_3 /WO_{3-x}, it is found that Na ions preferentially diffuse along the twin boundaries [38]. Our simulation directly predict that a thin-layer twin wall can act as a fast channel for vacancy diffusion. The enhanced diffusion along twin boundaries is quite similar to pipe diffusion in dislocation cores in FCC metals [69].

5 Conclusion

In summary, interactions between vacancies and twin walls in ferroelastic materials have been investigated by combining MD and Monte Carlo simulations. Our findings can be summarized as follows:

(1) By applying a simple shear, a complex twin pattern is formed together with the formation of new domains with different orientations, and the nucleation and movement of kinks and junctions. The existence of vacancies facilitates the formation of twin patterns, resulting in an increase of the twin boundary density in comparison with that in vacancy-free samples.

(2) During mechanical shearing, vacancies prefer to bind with twin boundaries, kinks and junctions rather than staying in the bulk. Among all these defects, vacancies have the largest binding energy with junctions and migrate with the motion of junctions.

Twin boundaries provide weaker trapping sites. Once the twin boundaries start to move, the original trapped vacancies arranges in a straight line to form a “ghost line” since there is a delay for vacancies diffusing to the moving boundary.

(3) The thin-layer twin wall acts as a channel for fast diffusion. The diffusion coefficient can be enhanced around one order of magnitude in comparison to that of bulk diffusion.

(4) The vacancy concentration in twin boundaries increases with the increase of vacancy concentration in the whole system. The magnitude of this ratio is related to the vacancy diffusivity. After a long-time relaxation, the enrichment ratio converges to 0.5, which is the upper limit for estimating the vacancy concentration at twin boundaries for a given concentration in the system. The vacancy trapping ability of twin boundaries becomes weaker with increasing temperature, and eventually disappears at very high temperatures (thermally activated defects).

(5) Finally, we carried out the statistical analysis of the influence of vacancies on mechanical deformation. Their energy-drop distribution follows a power law, and the exponent increases from $\varepsilon \sim 1.44$ to 2.0 when the defect concentration increases. The exponent ε is the same in the athermal region. In addition, mobile vacancies raise the Vogel-Fulcher temperature slightly.

Acknowledgements

X. D and J. S appreciate the support of the Natural Science Foundation of China (51320105014, 51621063) and the 111 Project (No. BP 2018008). S.M.S. acknowledges support from the Research Council of Norway (231430). E.K.H.S. is grateful to the Engineering and Physical Sciences Research Council (EP/P024904/1) and the Leverhulme Foundation (RPG-2012-564) for support.

References

[1] L. Liu, X. Ding, J. Sun, S. Li, E.K.H. Salje, Breakdown of shape memory effect in bent Cu–Al-Ni nanopillars: when twin boundaries become stacking faults, Nano Lett. 16(1) (2016) 194-198.

[2] E. Hornbogen, Review thermo-mechanical fatigue of shape memory alloys, J. Mater. Sci. 39(2) (2004) 385-399.

[3] S. Li, X. Ding, J. Deng, T. Lookman, J. Li, X. Ren, J. Sun, A. Saxena, Superelasticity in bcc nanowires by a reversible twinning mechanism, Phys. Rev. B 82(20) (2010) 205435.

[4] S. Li, X. Ding, J. Li, X. Ren, J. Sun, E. Ma, High-efficiency mechanical energy storage and retrieval using interfaces in nanowires, Nano Lett. 10(5) (2010) 1774-1779.

[5] Y. Yang, S. Li, X. Ding, J. Sun, E.K.H. Salje, Interface driven pseudo-elasticity in a-Fe nanowires, Adv. Funct. Mater. 26(5) (2016) 760-767.

[6] R.J. Harrison, S.A.T. Redfern, E.K.H. Salje, Dynamical excitation and anelastic relaxation of ferroelastic domain walls in $LaAlO_3$, Phys. Rev. B 69(14) (2004) 144101.

[7] S. Kustov, I. Liubimova, E.K.H. Salje, $LaAlO_3$: A substrate material with unusual ferroelastic properties, Appl. Phys. Lett. 112(4) (2018) 042902.

[8] S. Kustov, S. Golyandin, K. Sapozhnikov, J. Van Humbeeck, R. De Batist, Low-temperature anomalies in Young's modulus and internal friction of Cu-Al-Ni single crystals, Acta Mater. 46(14) (1998) 5117-5126.

[9] S. Kustov, S. Golyandin, K. Sapozhnikov, E. Cesari, J.V. Humbeeck, R.D. Batist, Influence of martensite stabilization on the low-temperature non-linear anelasticity in Cu-Zn-Al shape memory alloys, Acta Mater. 50(11) (2002) 3023-3044.

[10] S. Kustov, K. Sapozhnikov, X. Wang, Phenomena associated with diffusion, assisted by moving interfaces in shape memory alloys: A review of our earlier studies, Funct. Mater. Lett. 10(01) (2017) 1740010.

[11] A.H. Cottrell, B.A. Bilby, Dislocation theory of yielding and strain ageing of iron, Proc. Phys. Soc.: A 62(1) (1949) 49-62.

[12] G. Fan, Y. Zhou, K. Otsuka, X. Ren, K. Nakamura, T. Ohba, T. Suzuki, I. Yoshida, F. Yin, Effects of frequency, composition, hydrogen and twin boundary density on the internal friction of $Ti_{50}Ni_{50-x}Cu_x$ shape memory alloys, Acta Mater. 54(19) (2006) 5221-5229.

[13] Y. Zhou, G. Fan, D. Xue, X. Ding, K. Otsuka, J. Sun, X. Ren, High damping capacity in a wide ambient-temperature range in hydrogen-doped and hydrogen-free Ti-45Pd-5Cr martensitic alloy, Scripta Mater. 61(8) (2009) 805-808.

[14] S. Kustov, J. Pons, E. Cesari, J. Van Humbeeck, Pinning-induced stabilization of martensite: Part II. Kinetic stabilization in Cu-Zn-Al alloy due to pinning of moving interfaces, Acta Mater. 52(10) (2004) 3083-3096.

[15] Q. Yang, S.L. Wang, J. Chen, T.N. Zhou, H.B. Peng, Y.H. Wen, Strong heating rate-dependent deterioration of shape memory effect in up/step quenched Cu-based alloys: A ductile CuAlMn alloy as an example, Acta Mater. 111 (2016) 348-356.

[16] X. Wang, J. Van Humbeeck, B. Verlinden, S. Kustov, Thermal cycling induced room temperature aging effect in Ni-rich NiTi shape memory alloy, Scripta Mater. 113 (2016) 206-208.

[17] S. Kustov, B. Mas, Z. Kuskarbaev, X. Wang, J. Van Humbeeck, Reply to comment on: “On the effect of room temperature ageing of Ni-rich NiTi alloys”, Scripta Mater. 123 (2016) 166-168.

[18] E.K.H. Salje, Multiferroic domain boundaries as active memory devices: trajectories towards

domain boundary engineering, ChemPhysChem 11(5) (2010) 940-950.
[19] S. Li, Y. Li, Y. Lo, T. Neeraj, R. Srinivasan, X. Ding, J. Sun, L. Qi, P. Gumbsch, J. Li, The interaction of dislocations and hydrogen-vacancy complexes and its importance for deformation-induced proto nano-voids formation in α-Fe, Int. J. Plasticity 74 (2015) 175-191.
[20] T. Rojac, M. Kosec, B. Budic, N. Setter, D. Damjanovic, Strong ferroelectric domain-wall pinning in $BiFeO_3$ ceramics, J. Appl. Phys. 108(7) (2010) 074107.
[21] E.K.H. Salje, S.A. Hayward, W.T. Lee, Ferroelastic phase transitions: structure and microstructure, Acta Crystallogr. Sect. A 61(1) (2005) 3-18.
[22] E.K.H. Salje, W.T. Lee, Pinning down the thickness of twin walls, Nature Mater. 3 (2004) 425-426.
[23] S.A. Hayward, E.K.H. Salje, Twin memory and twin amnesia in anorthoclase, Mineral. Mag. 64(2) (2000) 195-200.
[24] L. Goncalves-Ferreira, S.A.T. Redfern, E. Artacho, E.K.H. Salje, W.T. Lee, Trapping of oxygen vacancies in the twin walls of perovskite, Phys. Rev. B 81(2) (2010) 024109.
[25] M. Calleja, M.T. Dove, E.K.H. Salje, Trapping of oxygen vacancies on twin walls of $CaTiO_3$: a computer simulation study, J. Phys.: Condens. Matter 15(14) (2003) 2301-2307.
[26] A. Angoshtari, A. Yavari, Effect of strain and oxygen vacancies on the structure of 180° ferroelectric domain walls in $PbTiO_3$, Comput. Mater. Sci. 48(2) (2010) 258-266.
[27] G.C. Mather, M.S. Islam, F.M. Figueiredo, Atomistic study of a $CaTiO_3$-based mixed conductor: defects, nanoscale clusters, and oxide-ion migration, Adv. Funct. Mater. 17(6) (2007) 905-912.
[28] I.S. Vorotiahin, A.N. Morozovska, Y.A. Genenko, Hierarchy of domain reconstruction processes due to charged defect migration in acceptor doped ferroelectrics, arXiv preprint arXiv:1907.02580 (2019).
[29] X. He, E.K.H. Salje, X. Ding, J. Sun, Immobile defects in ferroelastic walls: Wall nucleation at defect sites, Appl. Phys. Lett. 112(9) (2018) 092904.
[30] J. Seidel, P. Maksymovych, Y. Batra, A. Katan, S.Y. Yang, Q. He, A.P. Baddorf, S.V. Kalinin, C.H. Yang, J.C. Yang, Y.H. Chu, E.K.H. Salje, H. Wormeester, M. Salmeron, R. Ramesh, Domain wall conductivity in La-doped $BiFeO_3$, Phys. Rev. Lett. 105(19) (2010) 197603.
[31] T. Rojac, A. Bencan, G. Drazic, N. Sakamoto, H. Ursic, B. Jancar, G. Tavcar, M. Makarovic, J. Walker, B. Malic, D. Damjanovic, Domain-wall conduction in ferroelectric $BiFeO_3$ controlled by accumulation of charged defects, Nature Mater. 16(3) (2017) 322-327.
[32] V. Nagarajan, A. Roytburd, A. Stanishevsky, S. Prasertchoung, T. Zhao, L. Chen, J. Melngailis, O. Auciello, R. Ramesh, Dynamics of ferroelastic domains in ferroelectric thin films, Nature Mater. 2 (2002) 43-47.
[33] J.F. Scott, E.K.H. Salje, M.A. Carpenter, Domain wall damping and elastic softening in $SrTiO_3$: Evidence for polar twin walls, Phys. Rev. Lett. 109(18) (2012) 187601.
[34] S. Van Aert, S. Turner, R. Delville, D. Schryvers, G. Van Tendeloo, E.K.H. Salje, Direct observation of ferrielectricity at ferroelastic domain boundaries in $CaTiO_3$ by electron microscopy, Adv. Mater. 24(4) (2012) 523-527.
[35] L. He, D. Vanderbilt, First-principles study of oxygen-vacancy pinning of domain walls in $PbTiO_3$, Phys. Rev. B 68(13) (2003) 134103.
[36] A. Aird, M.C. Domeneghetti, F. Mazzi, V. Tazzoli, E.K.H. Salje, Sheet superconductivity in : crystal structure of the tetragonal matrix, J. Phys.: Condens. Matter 10(33) (1998) L569-L574.
[37] Y. Kim, M. Alexe, E.K.H. Salje, Nanoscale properties of thin twin walls and surface layers in

piezoelectric WO_{3-x}, Appl. Phys. Lett. 96(3) (2010) 032904.
[38] A. Aird, E.K.H. Salje, Enhanced reactivity of domain walls in with sodium, Eur. Phys. J. B 15(2) (2000) 205-210.
[39] J.F. Scott, M. Dawber, Oxygen-vacancy ordering as a fatigue mechanism in perovskite ferroelectrics, Appl. Phys. Lett. 76(25) (2000) 3801-3803.
[40] H.N. Al-Shareef, D. Dimos, T.J. Boyle, W.L. Warren, B.A. Tuttle, Qualitative model for the fatiguefree behavior of $SrBi_2Ta_2O_9$, Appl. Phys. Lett. 68(5) (1996) 690-692.
[41] Q.F. Fang, R. Wang, Atomistic simulation of the atomic structure and diffusion within the core region of an edge dislocation in aluminum, Phys. Rev. B 62(14) (2000) 9317-9324.
[42] R.C. Picu, D. Zhang, Atomistic study of pipe diffusion in Al–Mg alloys, Acta Mater. 52(1) (2004) 161-171.
[43] M. Legros, G. Dehm, E. Arzt, T.J. Balk, Observation of giant diffusivity along dislocation cores, Science 319(5870) (2008) 1646-1649.
[44] E.K.H. Salje, X. Ding, Z. Zhao, T. Lookman, A. Saxena, Thermally activated avalanches: Jamming and the progression of needle domains, Phys. Rev. B 83(10) (2011) 104109.
[45] X. Ding, Z. Zhao, T. Lookman, A. Saxena, E.K.H. Salje, High junction and twin boundary densities in driven dynamical systems, Adv. Mater. 24(39) (2012) 5385-5389.
[46] X. Ding, T. Lookman, Z. Zhao, A. Saxena, J. Sun, E.K.H. Salje, Dynamically strained ferroelastics: Statistical behavior in elastic and plastic regimes, Phys. Rev. B 87(9) (2013) 094109.
[47] S. Nosé, A unified formulation of the constant temperature molecular dynamics methods, J. Chem. Phys. 81(1) (1984) 511-519.
[48] W.G. Hoover, Canonical dynamics: Equilibrium phase-space distributions, Phys. Rev. A 31(3) (1985) 1695-1697.
[49] S. Plimpton, Fast parallel algorithms for short-range molecular dynamics, J. Comput. Phys. 117(1) (1995) 1-19.
[50] J. Li, AtomEye: an efficient atomistic configuration viewer, Modelling Simul. Mater. Sci. Eng. 11(2) (2003) 173-177.
[51] A. Stukowski, Visualization and analysis of atomistic simulation data with OVITO-the Open Visualization Tool, Modelling Simul. Mater. Sci. Eng. 18(1) (2010) 015012.
[52] T.D. Swinburne, S.L. Dudarev, S.P. Fitzgerald, M.R. Gilbert, A.P. Sutton, Theory and simulation of the diffusion of kinks on dislocations in bcc metals, Phys. Rev. B 87(6) (2013) 064108.
[53] J. Schaab, S.H. Skjærvø, S. Krohns, X. Dai, M.E. Holtz, A. Cano, M. Lilienblum, Z. Yan, E. Bourret, D.A. Muller, M. Fiebig, S.M. Selbach, D. Meier, Electrical half-wave rectification at ferroelectric domain walls, Nature Nanotech. 13(11) (2018) 1028-1034.
[54] S.H. Skjærvø, D.R. Småbråten, N.A. Spaldin, T. Tybell, S.M. Selbach, Oxygen vacancies in the bulk and at neutral domain walls in hexagonal $YMnO_3$, Phys. Rev. B 98(18) (2018) 184102.
[55] X. Li, Q. Yang, J. Cao, L. Sun, Q. Peng, Y. Zhou, R. Zhang, Domain wall motion in perovskite ferroelectrics studied by the nudged elastic band method, J. Phys. Chem. C 122(5) (2018) 3091-3100.
[56] J. Chrosch, E.K.H. Salje, Temperature dependence of the domain wall width in $LaAlO_3$, J. Appl. Phys. 85(2) (1999) 722-727.
[57] W.T. Lee, E.K.H. Salje, L. Goncalves-Ferreira, M. Daraktchiev, U. Bismayer, Intrinsic activation energy for twin-wall motion in the ferroelastic perovskite $CaTiO_3$, Phys. Rev. B 73(21) (2006) 214110.

[58] E.K.H. Salje, Ferroelastic Materials, Annu. Rev. Mater. Res. 42(1) (2012) 265-283.
[59] I. Stolichnov, M. Iwanowska, E. Colla, B. Ziegler, I. Gaponenko, P. Paruch, M. Huijben, G. Rijnders, N. Setter, Persistent conductive footprints of 109° domain walls in bismuth ferrite films, Appl. Phys. Lett. 104(13) (2014) 132902.
[60] M. Calleja, M.T. Dove, E.K.H. Salje, Trapping of oxygen vacancies on twin walls of $CaTiO_3$: a computer simulation study, J. Phys.: Condens. Matter 15(14) (2003) 2301-2307.
[61] E.K.H. Salje, M.A. Carpenter, High frequency elastic losses in $LaAlO_3$ and its importance for $LaAlO_3/SrTiO_3$ heterojunctions, Appl. Phys. Lett. 99(5) (2011) 051907.
[62] J. Mizusaki, I. Yasuda, J.I. Shimoyama, S. Yamauchi, K. Fueki, Electrical conductivity, defect equilibrium and oxygen vacancy diffusion coefficient of $La_{1-x}Ca_xAlO_{3-\delta}$ single crystals, J. Electrochem. Soc. 140(2) (1993) 467-471.
[63] X. He, X. Ding, J. Sun, E.K.H. Salje, Parabolic temporal profiles of non-spanning avalanches and their importance for ferroic switching, Appl. Phys. Lett. 108(7) (2016) 072904.
[64] L. Zhang, E.K.H. Salje, X. Ding, J. Sun, Strain rate dependence of twinning avalanches at high speed impact, Appl. Phys. Lett. 104(16) (2014) 162906.
[65] A. Clauset, C. Shalizi, M. Newman, Power-law distributions in empirical data, SIAM Rev. 51(4) (2009) 661-703.
[66] S. Kustov, S. Golyandin, K. Sapozhnikov, E. Cesari, J. Van Humbeeck, R. De Batist, Influence of martensite stabilization on the low-temperature non-linear anelasticity in Cu-Zn-Al shape memory alloys, Acta Mater. 50(11) (2002) 3023-3044.
[67] K. Sapozhnikov, S. Golyandin, S. Kustov, E. Cesari, Defect-assisted diffusion and kinetic stabilisation in Cu–Al–Be β_1' martensite, Mater. Sci. Eng.: A 481-482 (2008) 532-537.
[68] S. Kustov, R. Santamarta, E. Cesari, K. Sapozhnikov, V. Nikolaev, V. Fedorov, V. Krymov, J. Van Humbeeck, Mechanical Spectroscopy of Hyperstabilized Martensites, Solid State Phenom. 184 (2012) 355-360.
[69] R.W. Balluffi, On measurements of self-diffusion rates along dislocations in FCC Metals, Phys. Stat. Sol. (b) 42(1) (1970) 11-34.